J Mater Sci: Mater Med (2007) 18:1413–1421
DOI 10.1007/s10856-006-0068-z

The role of ammonium citrate washing on the characteristics of mechanochemical–hydrothermal derived magnesium-containing apatites

Chun-Wei Chen · Wojciech L. Suchanek · Pavel Shuk · Kullaiah Byrappa · Charles Oakes · Richard E. Riman · Kelly Brown · Kevor S. TenHuisen · Victor F. Janas

Received: 10 July 2005 / Accepted: 17 January 2006 / Published online: 6 February 2007

Abstract The role of citrate washing on the physical and chemical characteristics of magnesium-substituted apatites (HAMgs) was performed. HAMgs were synthesized by a mechanochemical–hydrothermal route at room temperature in as little as 1 h, which is five times faster than our previous work. Magnesium-substituted apatites had concentrations as high as 17.6 wt% Mg with a corresponding specific surface area (SSA) of 216 m^2/g. A systematic study was performed to examine the influence of increasing magnesium content on the physical and chemical characteristics of the reaction products. As the magnesium content increased from 0 to 17.6 wt%, magnesium-doped apatite crystallite size decreased from 12 to 8.8 nm. The Mg/(Mg + Ca) ratio in the product was enriched relative to that used for the reacting precursor solution. During mechanochemical–hydrothermal reaction, magnesium doped apatites co-crystallize with magnesium hydroxide. Citrate washing serves to remove the magnesium hydroxide phase. The concomitant increase in surface area results because of the removal of this phase. Possible mechanisms for magnesium hydroxide leaching are discussed to explain the measured trends.

C.-W. Chen (✉) · W. L. Suchanek · P. Shuk · K. Byrappa · C. Oakes · R. E. Riman
Department of Ceramic and Materials Engineering, Rutgers University, 607 Taylor Road, Piscataway, NJ 08854, USA
e-mail: c_wchen@hotmail.com

K. Brown · K. S. TenHuisen · V. F. Janas
Center for Biomaterials and Advanced Technologies, Medical Devices Group, a Division of Ethicon, Inc., Rt. 22 W, P. O. Box 151, Somerville, NJ 08876, USA

Present Address:
W. L. Suchanek
Sawyer Technical Materials, LLC, 35400 Lakeland Blvd., Eastlake, OH 44095, USA

Present Address:
P. Shuk
Rosemount Analytic INC., 1201 North Main Street, P. O. Box 901, Orrville, OH 4467-0901, USA

K. Byrappa
Department of Geology, University of Mysore, P. B. No. 21, Mysore 570006, India

Present Address:
K. S. TenHuisen
Reconstructive Business, Stryker Howmedica Osteonics, 59 Rt. 17 South, Allendale, NJ 07401, USA

1 Introduction

The development of new materials for the effective repair of the skeletal system has become a topic of interest [1, 2]. Synthetic hydroxyapatite (HA), $Ca_{10}(PO_4)_6(OH)_2$, has excellent biocompatibility with tooth and bone tissues and is frequently used as a biomaterial [3–5]. In vivo, HA grows in solutions that contain many essential trace elements besides calcium and phosphorus. Resultantly, biological apatites contain a number of trace elements, such as Mg^{2+}, Fe^{2+}, Na^+, CO_3^{2-}, F^-, Cl^- etc. [6]. The incorporation of these trace elements can affect the crystallinity, morphology, lattice constants, solubility and the stability of the resulting HA [7, 8]. Other than calcium, magnesium is the main bivalent cation found in biological apatites. Magnesium substitution on the HA lattice has been the subject of many studies concerned with the influence of this ion on

biological and synthetic apatites. Magnesium ions can catalyze certain bioreactions and is most likely a dental caries-promoting element released from enamel in the early stages of dental caries [9]. On the other hand, magnesium inhibits phase transformation from amorphous calcium phosphate to HA [10] and reduces the thermal stability of HA [11].

The development of new synthesis techniques for magnesium-containing apatite (HAMg) with controlled chemical composition and morphology is of great importance from the scientific and technological viewpoint. Mayer et al. [12] reported the synthesis of uniform doped apatites containing biologically relevant amounts of Mg (0.2–1.5%) by mixing $Ca(NO_3)_2$, $Mg(NO_3)_2$, and Na_2HPO_4 solutions. Other workers have reported the effect of Mg on the morphology and lattice constants of apatites prepared by precipitation at relatively higher magnesium concentrations [13, 14]. Bigi et al. [13] found that the degree of magnesium substitution for calcium in the apatite structure can be at most ~10 atom% and excess magnesium is located in the amorphous phase and/or on crystallite surfaces. Yasukawa and coworkers prepared magnesium–calcium apatites by a wet method from aqueous solutions with Mg contents ranging from 0 to 50 atom% using $Mg(NO_3)_2$, $Ca(OH)_2$, and H_3PO_4 as the starting materials [14]. It was found that the particles became less crystalline with increasing Mg content and the products were amorphous above 31 atom% Mg. Recently, other workers have also reported the formation of amorphous phases at higher magnesium concentrations when HAMg materials were produced by different methods [15–17]. Okazaki et al. synthesized HAMg at 80°C by precipitation from calcium acetate, magnesium acetate and ammonium dihydrogen phosphate solutions [18]. They reported that the solubility at 37°C in 0.5 M acetate buffer solution of pH 4.0 increased with increasing Mg concentration.

In our previous work, we have reported the synthesis of stoichiometric crystalline HA powder from the heterogeneous reaction of $Ca(OH)_2$ powder and $(NH_4)_2HPO_4$ solution by the mechanochemical–hydrothermal (M–H) method [19, 20]. It was verified that water actively participates in the synthesis by dissolving one of the reacting powders as well as serves as a reactant to produce a highly crystalline HA. In particular, the mechanochemical–hydrothermal route is a novel methodology able to produce large quantities of nanostructured apatite reproducibly with controlled composition and phase purity. Furthermore, we presented emulsion-based methods as means to prepare highly dispersible apatite nanopowders [21].

Recently, we also demonstrated that HAMg powders with different crystallinity levels could be prepared from the heterogeneous reaction between $Mg(OH)_2/Ca(OH)_2$ powders and $(NH_4)_2HPO_4$ solution via the M–H route [22]. This work showed the concentration of Mg in hydroxyapatite can achieve levels higher than ever previously reported. However, Mg-substitution in calcium phosphates do not remain as hydroxyapatite when heat-treated at 900°C, which is why these magnesium substituted compounds are referred to as apatites. Instead, Mg-substituted calcium phosphates decompose to a complex phase mixture whose composition depending on the level of magnesium substitution examined. Mg-substituted β-tricalcium phosphate ($(Mg, Ca)_3(PO_4)_2$, aka., β-TCMP) is commonly observed as one of the many phases typically observed [11]. Our previous work also utilized long 5 h reaction times and detailed characterization of the citrate washing step was not reported. This paper will describe a new procedure that reduces this processing time and report more details concerning the physical and chemical characteristics of the magnesium doped apatites as a function of magnesium content and citrate washing.

2 Experimental procedure

2.1 Synthesis of HAMg powders

The preparation of HAMg powders at different magnesium contents by the mechanochemical–hydrothermal method is similar to that of stoichiometric HA, as described in detail elsewhere [20]. The samples prepared in the presence of 10, 20, 30, 50 mol% of Mg in the slurries, with respect to the total molar fraction of alkaline earth metal (Mg/(Mg + Ca)), are named HAMg10, HAMg20, HAMg30 and HAMg50. For example, 22.07 g of calcium hydroxide ($Ca(OH)_2$, analytical grade, Alfa Aesar, Ward Hill, MA) and 4.37 g of magnesium hydroxide ($Mg(OH)_2$, analytical grade, Alfa Aesar, Ward Hill, MA) powders were suspended in 200 mL of deionized water (18.2 MΩ cm resistivity, Millipore RiOs and Elix water purification systems, Millipore Corporation, Burlington, MA). A stoichiometric amount of ammonium hydrogen phosphate ($(NH_4)_2HPO_4$, 29.41 g, analytical grade, Alfa Aesar, Ward Hill, MA) was dissolved in 150 mL of deionized water. The $(NH_4)_2HPO_4$ solution was added slowly to $Ca(OH)_2/Mg(OH)_2$ suspension while vigorously stirring with a magnetic stirrer. The presence of water adsorbed and other volatile components on all

reactants was measured by thermogravimetric analysis to maintain the targeted chemical compositions, which are listed in Table 1 as mole fractions. For example, for HAMg20, the (Ca + Mg)/P molar ratio in the starting slurry was 1.67 and the Mg content was 0.2 (20 mol%).

A multi-ring media mill equipped with a zirconia liner and zirconia ring grinding media (Model Micros MIC-0, Nara Machinery Co., Tokyo, Japan) was used to synthesize HAMg powders. A jacketed water-cooling system was used to keep the reaction temperature in the range of 22–32°C. The mechanochemical reaction of the slurry was carried out in air, initially at a rotation speed of 1,000 rpm for 12 min and then at 2,000 rpm for 48 min. The temperature during the grinding measured with a thermocouple ranged between 19 and 22°C at 1,000 rpm and 25–32°C at 2,000 rpm depending upon the batch. After mechanochemical–hydrothermal syntheses, solid products were washed 3–6 times by shaking (Model 6000 Shaker, Eberbach Corporation, Ann Arbor, MI) in deionized water followed by centrifuging (Induction Drive Centrifuge, Model J2-21M, Beckman Instruments, Palo Alto, CA) at 5,000 rpm for 30 min. Early in our work, we observed that the drying method had a significant impact on the physical characteristics of powder. From previous work [19], conventional oven drying at 70°C for 24 h produces a powder with a specific surface area (SSA) of 90 m^2/g. By alternatively drying the powders with lyophillization, the SSA increased to 175 m^2/g. Powders that are lyophilized also show a reduction in the degree of agglomeration over those of conventional oven drying [20]. These results led us to utilize lyophillization for all samples produced in these studies. The washed powder was shell frozen and lyophilized (Model FO-20-85 BMP Freezer Dryer, FTS Systems, Inc., Stone Ridge, NY) for 50 h; and herein termed as ''as-prepared HAMg (HAMga).

2.2 Citrate washing

An ammonium citrate bath solution was prepared by adding ammonium hydroxide (reagent grade, Fisher Scientific, Pittsburgh, PA) into 0.2 M citrate acid (reagent grade, Aldrich, Milwaukee, WI) solution and the final pH of the solution was adjusted to 8.9. One part of as-prepared HAMg was added into the citrate bath (100 mL per 1 g of dried powder). The suspension was stirred with a magnetic stirrer overnight. And then, the product was separated from the solution by centrifugation and washed by deionized water by 5–6 cycles of shaking and centrifuging**.** The citrate bath treated product was lyophilized and termed as ''citrate-treated'' HAMg or HAMgb. In order to check thermal stability of the HAMgb samples, a small quantity of each products were placed in an alumina crucible and heat treated in air at 900°C for 1 h; hereon named as ''heat-treated'' HAMgb (HAMgbc).

2.3 Characterization

Chemical analyses for Ca, Mg and P in as-prepared HA and citrate-treated HAMg samples were accomplished by X-ray fluorescence spectroscopy (Oneida Research Services, Inc., Whitesboro, NY). The XRD analyses were carried out by a Kristalloflex D-500 powder diffractometer using Ni filtered Cu Kα radiation. The samples were scanned in the 2θ range of 10–70°, at a step size of 0.05 (°/step). Crystallographic identification of the as-prepared, citrate-treated, and heat-treated HAMg powders was accomplished by comparing the experimental XRD patterns to standards compiled by the International Committee for Diffraction Data (ICDD; HA, card #09-0432; β-TCP, #09-0169; CaO, #37-1497; $Mg(OH)_2$, #07-0239). When

Table 1 Preparation conditions and properties of apatite samples

Preparation condition[a]				Mg content[b]	SSA[c] (m^2/g)		d^{d}_{BET}(nm)
Sample	$Mg(OH)_2$ mol	$Ca(OH)_2$ mol	Mg/(Mg + Ca)	Mg (wt%)	As-prepared	Citrate-treated	Citrate-treated
HA	0.000	0.337	0	0.0	174 ± 5	157 ± 4	12.0
HAMg10	0.033	0.297	0.1	2.1	22 ± 4	168 ± 6	11.2
HAMg20	0.074	0.297	0.2	6.6	45 ± 10	181 ± 12	10.5
HAMg30	0.110	0.256	0.3	15.1	67 ± 5	238 ± 7	8.0
HAMg50	0.175	0.175	0.5	17.6	107 ± 8	216 ± 10	8.8

[a] The amount of $(NH_4)_2HPO_4$ used to prepare the slurry changed from 0.2 to 0.22 mol in order to keep Ca/P or (Ca + Mg)/P molar ratio = 1.67

[b] Chemical analysis results of as-prepared HA and citrate-treated HAMg samples

[c] SSA denotes the specific surface area from BET measurement

[d] d_{BET} denotes the equivalent spherical diameter

HA and Mg-substituted β-tricalcium phosphate two-phase mixtures were found, the phase composition was estimated with quantitative XRD methods. Mixtures consisting of HA (reagent grade, Sigma-Aldrich, St. Louis, MO) and β-TCP (reagent grade, Fluka, Switzerland) of known concentrations were prepared using a mortar and pestle for homogenization. Standard mixtures were prepared corresponding to 20, 40, 60, and 80 wt% β-TCP in HA. XRD scans performed at the conditions cited above were used to obtain a calibration curve where the ratio of the integrated intensity ratio of (2 1 1) reflections for HA ($2\theta = 31.8^{o}$) to (0 2 10) reflections for β-TCP ($2\theta = 31^{o}$) were plotted as a function of phase composition. By measuring the integrated intensity ratio for the experimental samples of unknown phase concentration, the calibration curve was used to estimate the phase composition. No corrections were made for the β-TCP or HA standards to correct for changes in absorption coefficient, which would be attributed to substitution of calcium by magnesium. Thus, the concentrations reported in this work were considered semi-quantitative estimates.

The specific surface area (SSA) was measured via BET analysis of nitrogen adsorption isotherms (Gemini III 2375 Surface Area Analyzer, Micromeritics Instrument Corporation, Norcross, GA). Particle size of the primary crystals was estimated from the nitrogen adsorption isotherms using the BET method to calculate equivalent spherical diameter d_{BET} from the following equation: $d_{BET} = 6/(\rho \cdot SSA)$, where ρ is particle density. A density of 3.156 g/cm^3, which is the theoretical density of stoichiometric HA, was used for all calculations. Transmission Electron Microscopy (TEM) images were obtained with a high-resolution analytical electron microscope (model EM-002B, International Scientific Instruments, Pleasanton, CA) at an acceleration voltage of 200 kV. The specimens were prepared by slow evaporation of a drop of the sample suspension deposited onto a copper grid with a carbon film. Transmission infrared (IR) spectra were recorded using a Perkin Elmer 1720-X Fourier Transform Infra-Red (FTIR) spectrometer. The apatite powder was ground with KBr in the proportion of 1/150 (by weight) for 10 min and pressed into a 3 mm pellet using a hand press (Qwik Handi-Press, Model 0016-125, Spectra-Tech, Inc., Shelton, CT). Thermal gravimetric analysis (TGA) and differential thermal analysis (DTA) were performed on Perkin- Elmer TGA-6 and DTA-7 thermal analyzers, respectively. Samples were heated at 5°C/min to a maximum temperature of 900°C under a N_2 atmosphere using a flow rate of 20 mL/min.

3 Results

From our previous report [22], magnesium-substituted apatite powders were prepared with a long reaction time of 5 h. In this case, the mechanical-hydrothermal reaction of the slurry was carried out initially at a rotation rate speed of 1,500 rpm for 1 h and then at 800 rpm for 4 h. However we chose to run the MIC-0 mill at conditions shown to be successful for making phase-pure hydroxyapatite [20]. The operating conditions for the MIC-0 correspond to 1,000 rpm for 12 min followed by 2,000 rpm for 48 min. Using this 1 h reaction sequence for processes incorporating magnesium led to form the same as-prepared phase assemblages as those observed for the 5 h reaction sequence. Chemical analysis of the apatites indicated that the Ca/P ratio of HA sample was 1.66, which was close to the Ca/P ratio of 1.67 in the starting slurry. Thus, for all HAMg preparation, the Mg/(Mg + Ca) ratio was chosen to vary from 0.1 to 0.5 while maintaining the (Ca + Mg)/P molar ratio to a constant value of 1.67.

The experimental conditions and corresponding calcium and magnesium chemical analyses for HA and HAMg powders are summarized in Table 1. The magnesium content increased from 2.1 to 17.6 wt% as the precursor Mg/(Mg + Ca) ratio was increased from 0.1 to 0.5. After mechanochemical–hydrothermal and citrate washing, the magnesium found in the HAMgb samples was directly proportional to the magnesium input in the slurry. On a molar basis, the proportionality factor for the ratio Mg/(Mg + Ca) for the washed powder to that of the precursor solution was found to be 1.7. Thus, the magnesium content in the final product is higher than that of the precursor slurry. These magnesium contents observed for the 1 h reaction were comparable to those measured for 5 h products [22]. Thus, from these results, we can conclude that the phase purity and chemical stoichiometry are not significantly affected by the short mechanochemical–hydrothermal reaction time.

The chemical characteristics of apatite powders produced by mechanochemical–hydrothermal treatments are affected by both the magnesium concentration in the precursor and the citrate washing step. This was studied with XRD, FTIR and thermal analysis. Figure 1 shows the XRD patterns of as-prepared HAa and HAMga samples with different Mg contents. The XRD pattern of the compound synthesized without Mg showed only one crystalline phase, namely HA (ICDD card #09-0432). However, unreacted $Mg(OH)_2$ was also present for all samples where Mg-substitution was attempted. The $Mg(OH)_2$ was also detected with

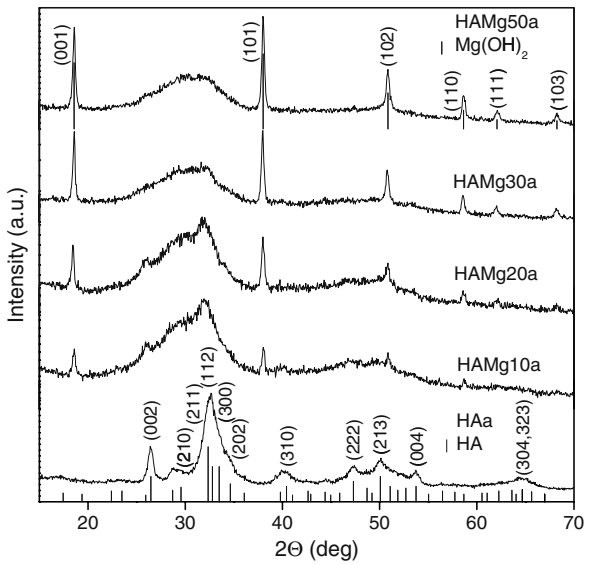

Fig. 1 XRD patterns of as-prepared apatite samples with different magnesium contents

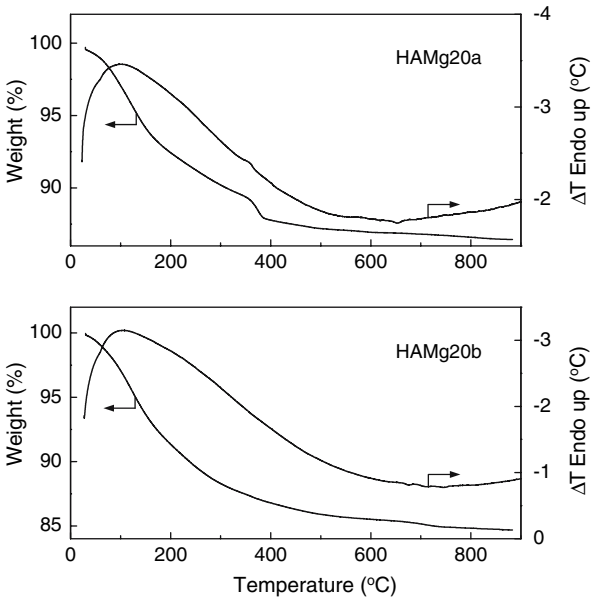

Fig. 3 TGA–DTA curves of as-prepared (HAMg20a) and citrate-treated (HAMg20b) samples

infrared spectroscopy and thermal analysis. For example, the infrared spectra of an as-prepared HAMg20 sample is shown in Fig. 2. A sharp peak at 3,698 cm^{-1} was observed and assigned as OH^- ions attributed to crystalline $Mg(OH)_2$ [23]. The TGA curve of HAMg20a shown in Fig. 3 exhibits a weight loss from 360 to 390°C due to the decomposition of $Mg(OH)_2$. The endothermal peak at ca. 370°C in the DTA curve of HAMg20a corresponds to the decomposition of $Mg(OH)_2$. Thermal gravimetric analysis of pure $Mg(OH)_2$ shows similar decomposition behavior with its weight loss initiated at 350°C and completed by 400°C. Heat-treating unwashed HAMg20a at 400°C for 1 h was also observed to remove the 3,698 cm^{-1} band, further confirming the interpretation of the infrared and thermal analysis data.

Figure 4 shows the XRD patterns of citrate-treated HAb and HAMgb samples. Examining diffraction patterns for unwashed and washed apatites (Figs. 1 and 4), the similarity of these diffractograms indicate that citrate bath washing does not decompose apatite, whether it is pure or Mg-doped apatite. Most importantly, the absence of $Mg(OH)_2$ diffraction peaks for

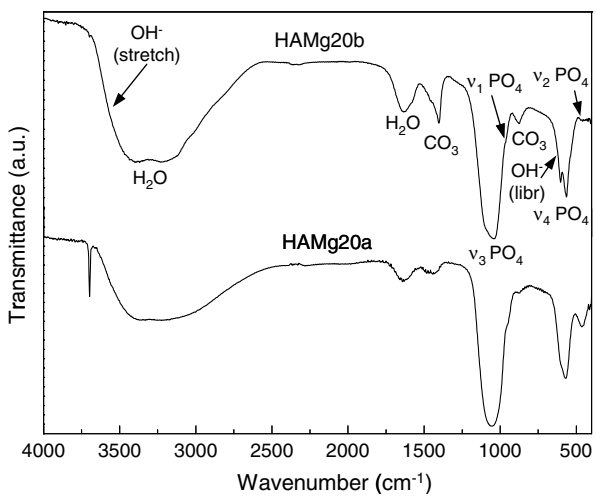

Fig. 2 FTIR spectra of as-prepared and citrate-treated HAMg20 samples

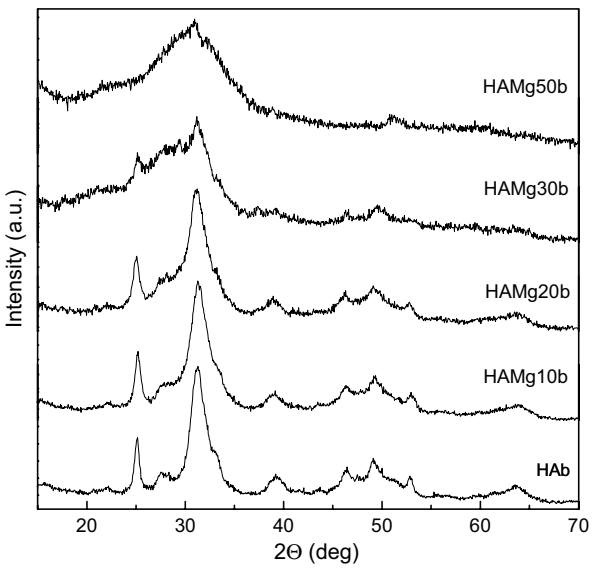

Fig. 4 XRD patterns of citrate-treated apatite samples with different magnesium contents

the magnesium doped samples indicates that $Mg(OH)_2$ was removed during citrate bath wash. Infrared spectroscopy shown in Fig. 2 supports the XRD data since no bands characteristic of $Mg(OH)_2$ are observed in the spectrum of HAMg20b sample. This is further supported by thermal analysis data since no weight loss was observed in the 400°C range for HAMg20b (Fig. 3). These results support the XRD and infrared data, which indicate that Mg in the precursor slurry partitioned into both the apatite structure and $Mg(OH)_2$. Subsequent citrate washing removes all detectable $Mg(OH)_2$.

Citrate washing also introduced some other unexpected chemical characteristics to the magnesium-doped apatite powders. The unwashed HAMg20 powders, shown in Fig. 2, exhibit two ν_4 PO_4 bands at 603 and 566 cm^{-1} as one broad peak. After washing, the broad ν_4 PO_4 band at 580 cm^{-1} is split into 603 and 566 cm^{-1} bands, as shown for the spectrum of HAMg20b. This broadening might be due to the phosphate species associated with Mg and those associated with Mg-doped apatite. In addition, the intensity of the 1,420 and 875 cm^{-1} bands increases relative to the as-prepared sample, which is associated with the incorporation of carbonate anions. This may be attributed to the use of pH 8.9 citrate wash solutions since basic pH promotes the absorption of atmospheric CO_2 into solution and subsequent reaction with base ions to form carbonate anions, which substitute into the apatite lattice.

XRD studies of the heat-treated washed magnesium-doped apatite powders show that they are thermally unstable. The stoichiometric HA (Ca/P = 1.67) is characterized by very high thermal stability. However, it is well known that small deviations from the ideal proportion of cations and anions severely degrade its thermal stability [24]. Representative XRD patterns of heat-treated HAbc and HAMg10bc samples are shown in Fig. 5. Heat treatment of pure washed hydroxyapatite (HAbc) led to XRD peaks associated with pure HA, as expected. In contrast, HAMg10bc showed the simultaneous presence of HA and β-TCP. The XRD peaks of β-TCP are shifted slightly towards higher diffraction angle as compared to pure β-TCP. This may be due to the incorporation of Mg into the crystal structure of β-TCP to give Mg-substituted β-tricalcium phosphate, $(Mg, Ca)_3(PO_4)_2$, (β-TCMP) [11]. The presence of magnesium reduces the thermal stability of apatites and favors its thermal transformation into β-TCMP. The weight fraction of β-TCMP increased slightly with measured Mg content in the HAMg sample. The measured β-TCMP contents of 62.6 and 67.8 wt% correspond to measured concentrations of 2.1

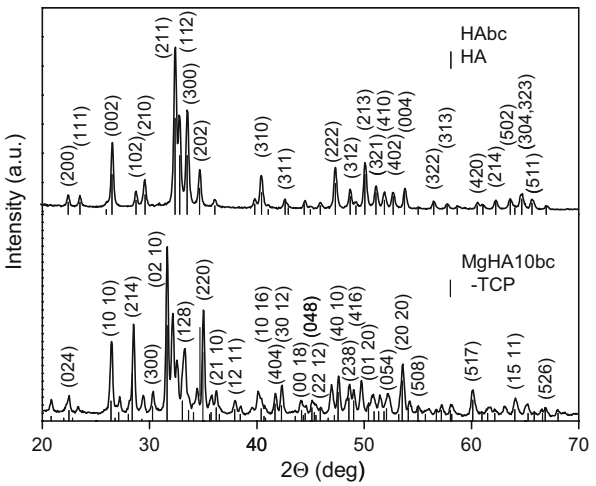

Fig. 5 XRD patterns of HAbc and MgHA10bc. Heat-treatment conditions: 900°C, in air, 1 h

and 6.6% Mg for HAMg10bc and HAMg20bc, respectively. Thus, the increase in β-TCMP is not proportional to the difference in magnesium concentration. Most likely, appreciable concentrations of Mg exist in the apatite phase. When the as-prepared HAMg10a sample was heat-treated at 900°C for 1 h, XRD analysis showed that the percentage of β-TCMP for HAMg10ac increased to 74.7 wt%. This large increase of β-TCMP over that of the washed HAMg10bc sample is an indication that significant concentrations of $Mg(OH)_2$ can be found in unwashed powders.

The physical characteristics of the magnesium-doped apatite powders are significantly affected by both the magnesium content and citrate washing. The specific surface area (SSA) values of as-prepared and citrate-treated HA and HAMg samples are plotted as a function of Mg content in Fig. 6. The SSA values of the as-prepared HAMg (HAMga) samples range from 22 to 107 m^2/g. The SSA of the as-prepared HAMga

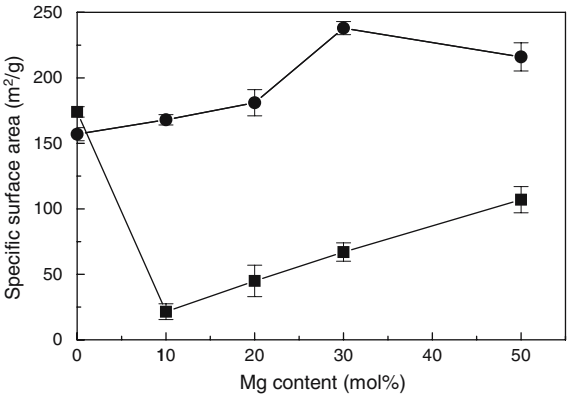

Fig. 6 Specific surface areas of as-prepared (■) and citrate-treated (•) apatites as a function of Mg content

sample was lower than that of HAa but increased with increasing Mg content. However, the SSA increased significantly after the citrate bath treatment, for all samples but pure hydroxyapatite. Pure HA was observed to reduce in SSA from 174 to 157 m^2/g when subjected to citrate washing. The SSA increased from 168 to 238 m^2/g when Mg content increased from 2.1 to 15.1 wt% and thereafter decreased slightly to 216 m^2/g for HAMg50b. The increase in SSA with increasing magnesium concentration for washed or unwashed samples is attributed to reductions in crystallite size. This is suggested by the increasing line broadening of XRD peaks with increasing magnesium concentration. This is particularly well pronounced when HAMg10b and HAM20b are compared to high magnesium containing HAMg30b and HAM50b. Based on SSA data, estimated crystallite sizes range from 12 to 8.8 for a corresponding concentration of magnesium ranging from 0 to 17.6 wt%.

Pure hydroxyapatite (HAa) and magnesium doped apatites, HAMg20a and HAMg20b, were studied with TEM to better understand the importance of citrate washing. Agglomerated or aggregated nanocrystallites in the range of 10–35 nm can be seen in the TEM image for the as-prepared unwashed HA sample (Fig. 7a), which is consistent with estimated diameters from SSA data. The as-prepared magnesium containing apatite (HAMg20a) consists of agglomerated/aggregated 25 nm particles (Fig. 7b). When HAMg20a is citrate washed to form HAMg20b, a smaller crystallite size is revealed (Fig. 7c). This is supported by SSA data where the estimated crystallite size is 10.5 nm. The high-resolution TEM (HRTEM) image shows that the HAMg20b sample possesses small HAMg crystals that are both highly crystalline and pure (Fig. 7d).

4 Discussion

Chemical characterization shows that mechanochemical–hydrothermal reactions produce a phase mixture of magnesium doped apatite and magnesium hydroxide. When citrate washing is implemented, magnesium hydroxide is removed and all that is left remaining is a magnesium-doped apatite. As increasing amounts of magnesium is doped into apatite, the crystallite size reduces, which explains both the XRD line broadening and SSA data. The consistent SSA increase of the

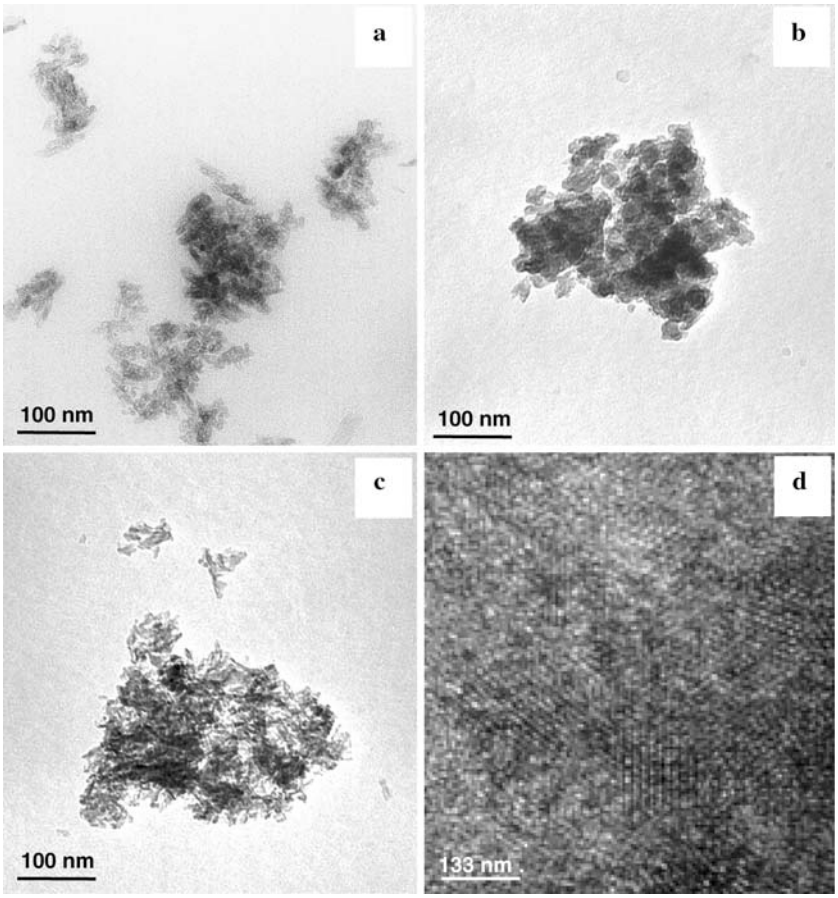

Fig. 7 TEM images of apatite samples with different magnesium contents: (**a**) HAa; (**b**) HAMg20a; (**c**) HAMg20b; (**d**) HAMg20b

HAMg powders after citrate washing suggests that a soluble phase is selectively leached from the particulate structure while leaving some type of skeletal network intact. Thus, it is possible that the as-prepared powders consist of an interpenetrating network of magnesium doped apatite and $Mg(OH)_2$. As citrate washing proceeds, the network of $Mg(OH)_2$ can be completely removed while leaving the magnesium doped apatite network intact. Such nanostructured leaching processes are well known for materials such as Vycor^{TM} [25]. Another possible explanation is that a phase mixture consisting of nanostructured magnesium doped apatite and coarser $Mg(OH)_2$ particles formed. With increasing amounts of magnesium, the particle size of the magnesium doped apatite decreases to increase surface area and decrease particle size. Upon washing these materials, the coarser $Mg(OH)_2$ particles dissolve to increase the surface area. Unfortunately, the TEM data is unable to distinguish between these two possible limiting scenarios. The decrease in SSA for pure hydroxyapatite upon citrate washing is no anomaly. In this case, this is attributed to finer particles dissolving faster than coarser particles. The small reduction in SSA observed here probably occurs to some extent in the magnesium doped apatites but because of the large increase in SSA resulting from $Mg(OH)_2$ leaching, this effect is secondary and hence not noticeable. It is possible that dissolution of small magnesium doped apatites might be dominant in the highest magnesium content sample (HAMg50), which might explain why the surface area of this sample is less than that found for HAMg30. The consistent enrichment of the Mg/(Mg + Ca) in the powders relative to that of the initial precursor reaction media suggests that either magnesium is preferentially crystallizing into the apatite lattice or calcium is selectively leached from the magnesium doped apatite lattice during citrate washing. Detailed chemical analysis of the calcium and magnesium concentration in both powders and supernatant for each stage of the synthesis process will be necessary to determine the likely mechanism of magnesium enrichment.

5 Conclusions

Mg-substituted apatites with magnesium content between 2.1 and 17.6 wt% were prepared by the mechanochemical–hydrothermal method at room temperature in as little as 1 h. Magnesium was partly incorporated into the apatite structure while $Mg(OH)_2$ precipitated as a second phase, which could be selective leached with citrate washing. The crystallite size of the magnesium doped apatites decreased with increasing Mg content. Upon heat-treatment at 900°C for 1 h, a phase mixture of apatite and Mg-substituted β-tricalcium phosphate resulted.

Acknowledgments This research was supported by the Johnson & Johnson Center for Biomaterials and Advanced Technologies, the Center for Biomedical Devices at Rutgers University, and the National Institute of Health.

References

1. C. REY, in ''Calcium Phosphates in Biological and Industrial Systems'', edited by Z. AMJAD, Kluwer Academic Publishers, Boston, 1998 p. 217
2. E. BERTONI, A. BIGI, G. COJAZZI, M. GANDOLFI, S. PANZAVOLTA and N. ROVERI, *J. Inorg. Biochem.* **72** (1998) 29
3. H. AOKI, (1991) Science and medical applications of hydroxyapaptite. Tokyo: Japanese Association of Apatite Science, p. 1
4. K. De GROOT, in ''Bioceramics of calcium phosphate'', edited by K. DE GROOT, CRC Press, Roca Raton, 1983, p. 131
5. J. C. ELLIOTT, (1994) Structure and chemistry of the apatites and other calcium orthophosphates. Amsterdam: Elsevier, p. 111
6. R. Z. LeGEROS, (1991) ''Monographs in Oral Science'' edited by H. M. MYERS, vol. 15. Karger, Basel, p. 46
7. A. BIGI, E. FORESTI, R. GREGORINI, A. RIPAMONTI, N. ROVERI and J. S. SHAH, *Calcif. Tissue Int.* **50** (1992) 439
8. W. G. M. Van Den HOEK, T. P. FEENSTRA and P. L. De BRUYN, *J. Phys. Chem.* **84** (1980) 3312
9. A. S. HALLSWORTH, C. ROBINSON and J. A. WEATHERELL, *Caries Res.* **7** (1973) 345
10. T. P. FEENSTRA, J. HOP and P. L. DEBRUYN, *J. Colloid Interface Sci.* **83** (1981) 583
11. A. BIGI, G. FALINI, E. GORESTI, M. GAZZANO, A. RIPANONTI and N. ROVERI, *J. Inorg. Biochem.* **49** (1993) 69
12. I. MAYER, R. SCHLAM and F. D. B. FEATHERSTONE, *J. Inorg. Biochem.* **66** (1997) 1
13. A. BIGI, G. FALINI, E. FORESTI, M. GAZZANO, A. RIPAMONTI and N. ROVERI, *Acta Cryst.* **B52** (1996) 87
14. A. YASUKAWA, S. OUCHI, K. KANDORI and T. ISHIKAWA, *J. Mater. Chem.* **6** (1996) 1401
15. T. HANAZAWA, M. AIZAWA, F. S. HOWELL and K. ITATANI, *Phosphorus Res. Bull.* **9** (1999) 5
16. A. TAMPIERI, G. CELOTTI, E. LANDI and M. SANDRI, *Key Eng. Mater.* **254** (2004) 264
17. K. J. LILLEY, Y. GBURECK, J. C. KNOWLES, D. F. FARRAR and J. E. BARRALET, *J. Mater. Sci.: Mater. Med.* **16** (2005) 455
18. M. OKAZAKI, J. TAKAHASHI and K. KIMURA, *Caries Res.* **20** (1986) 324
19. P. SHUK, W. L. SUCHANEK, T. HAO, E. GULLIVER, R. E. RIMAN, M. SENNA, K. S. TENHUISEN and V. F. JANAS, *J. Mater. Res.* **16** (2001) 1231

20. C.-W. CHEN, C. S. OAKES, K. BYRAPPA, R. E. RIMAN, K. BROWN, K. S. TENHUISEN and V. F. JANAS, *J. Mater. Chem.* **14** (2004) 2425
21. C.-W. CHEN, R. E. RIMAN, K. BROWN, K. S. TENHUISEN and V. F. JANAS, *J. Crystal Growth* **270** (2004) 615
22. W. L. SUCHANEK, K. BYRAPPA, P. SHUK, R. E. RIMAN, V. F. JANAS and K. S. TENHUISEN, *Biomaterials* **25** (2004) 4647
23. R. A. NYQUIST and O. K. RONALD, (1971) Infrared spectra of inorganic compounds. New York: Academic Press, p. 235
24. A. TAMPIERI, G. CELOTTI, S. SPRIO and C. MINGAZZINI, *Mater. Chem. Phys.* **64** (2000) 54
25. S. SCHNEIDER, (1991) Ceramics and Glasses, Engineered Materials Handbook, Vol 4. ASM International, p. 427